

# Blind Facial Image Quality Enhancement using Non-Rigid Semantic Patches

Ester Hait and Guy Gilboa, *Member, IEEE*

**Abstract**—We propose to combine semantic data and registration algorithms to solve various image processing problems such as denoising, super-resolution and color-correction. It is shown how such new techniques can achieve significant quality enhancement, both visually and quantitatively, in the case of facial image enhancement. Our model assumes prior high quality data of the person to be processed, but no knowledge of the degradation model. We try to overcome the classical processing limits by using semantically-aware patches, with adaptive size and location regions of coherent structure and context, as building blocks. The method is demonstrated on the problem of cellular photography enhancement of dark facial images for different identities, expressions and poses.

**Index Terms**—Prior-based image enhancement, Similarity measures, Non-rigid registration, Denoising

## I. INTRODUCTION

IN the past decades, handling common image flaws has gradually improved with the use of more sophisticated image priors and models. Early methods used pixel-based statistics, such as smoothness [1], piecewise smoothness [2], total-variation [3], pixel correlation [4], or wavelet decomposition [5] for image reconstruction. In recent years, non-parametric patch-based methods, such as Nonlocal Means [6] and BM3D [7], exploited local and nonlocal self-similarities. Other patch-based, training-based methods were using Markov Random Fields [8] and dictionary learning [9]. Today's main state-of-the-art methods are based on square patches with little if any semantic context [10], [11], [12]. In recent years, using *generic* image priors has started to reach an optimality bound; for example, for super-resolution [13] and denoising [14]. For facial images, *facial priors* were then used to break this limit; for example, face hallucination [15], or image compression using K-SVD [16]. We propose an alternative concept of using large non-rigid patches with high semantic value.

Fig. 1 demonstrates our model and its underlying assumptions. We aim to use *non-rigid* processing of *semantic patches* of facial features, while preserving structure and context coherency, to overcome the classical processing limits. Given today's highly available mobile photography devices, our model assumes using *high-quality personal priors* but *no knowledge of the degradation model*. The degradation can involve noise following possible nonlinear processing, resolution reduction, a certain degree of motion blur and contrast and color changes. Our approach suggests to solve the problem indirectly by a mechanism which is invariant to low-to-moderate quality

reductions. We also assume that no matches of high quality (HQ) and low quality (LQ) data are available for learning. As there is no degradation model, one also cannot generate faithfully LQ images by degrading HQ images (e.g. adding noise to a clean image). Experimental results are demonstrated on the problem of dark cellular image enhancement.

### A. Related Work

Capel and Zisserman [17] observed that better learning is obtained when considering different facial regions, rather than the whole face, and that better representation is needed when handling high-detail facial regions that attract human attention. A separate PCA basis was learned for different key facial regions. Unlike our proposed method, they use linear PCA decomposition and training sets of *multiple* people.

Jia and Gong [18] performed face hallucination of a single modality (expression, pose and illumination) into a set of high-resolution images of different modalities, but used multiple people's images as priors. Interestingly, they deduced that hallucinating the same expression as in the test image was better than hallucinating other expressions.

Lee *et al.* [19] represented multiple-pose facial images as a low-dimensional appearance manifold in the image space, for video face recognition. The appearance manifold, learned from training, consisted of pose manifolds and their connectivity matrix, encoding transition probabilities between images.

Yu *et al.* [20] incrementally super-resolved 3D facial texture from video under changing light and pose, but used temporal information from sequential frames and a generic 3D face model. They also handled facial non-rigidity using a local region-based approach: using a match statistic to detect significant facial regions expression changes between frames.

Shih *et al.* [21] performed noise level estimation for denoising, by maximizing the joint noise probability across same-identity facial images of different noise levels. The estimated noise level can then be used for state-of-the-art denoising algorithms requiring it, such as BM3D.

Joshi *et al.* [22] were the first to suggest the use of "personal priors" to enhance a particular person's image, performing both global and face-specific corrections. They relied on the growing available datasets of personal images. Their algorithm derived its strength from using multiple same-identity example images, which, as they observed, can span a smaller space than that spanned by images of multiple people.

They performed global corrections of non-facial regions (such as deblurring, color and exposure corrections) using mean and basis vectors generated using PCA decomposition

E. Hait and G. Gilboa are with the Department of Electrical Engineering, Technion - Israel Institute of Technology, Technion City, Haifa, 32000, Israel. E-mail: etyhait@campus.technion.ac.il, guy.gilboa@ee.technion.ac.il

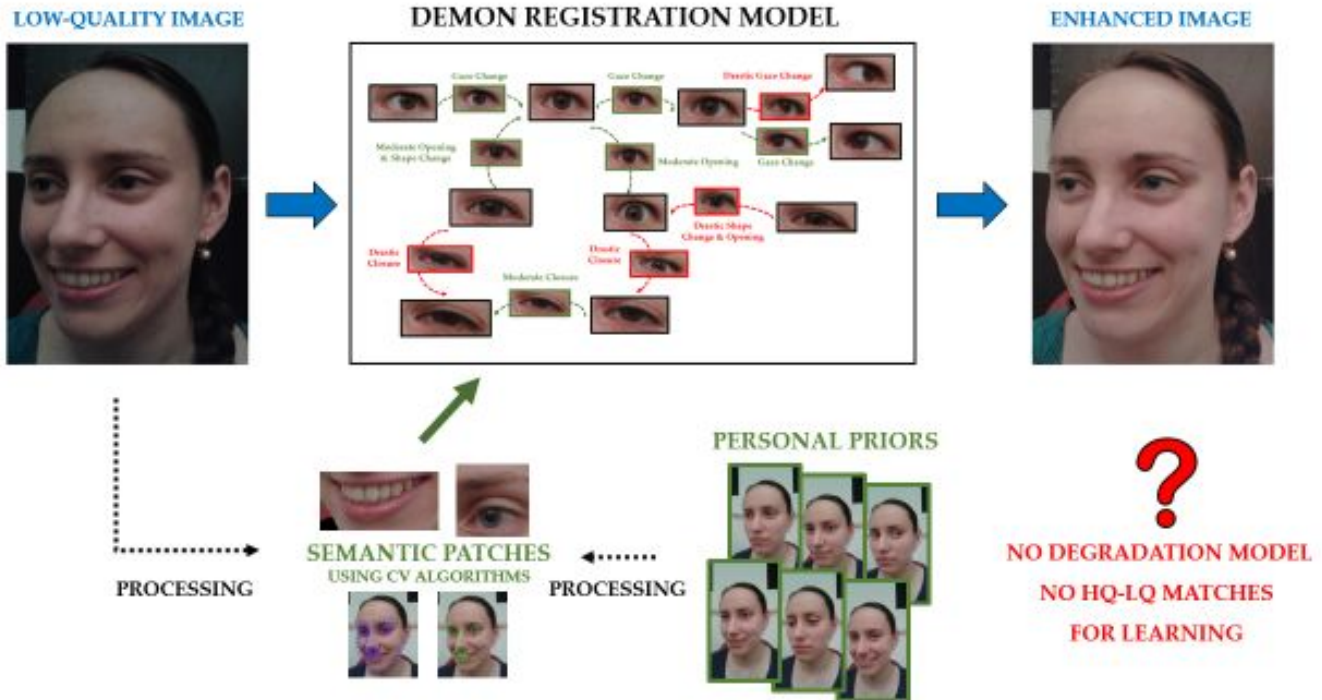


Fig. 1. Problem and assumptions of model: blind enhancement of low-quality facial images using prior data. Semantic patches of facial features are extracted to preserve structure and context coherency. Our model assumes available high-quality personal priors, but no knowledge of the degradation model and no matches of HQ and LQ data for learning.

(of every image layer) to derive priors for MAP estimation. They also performed local corrections of face regions (hallucination for sharpening; or inpainting for exposure correction), by transferring desired properties from HQ images in the gradient domain, using the Poisson equation.

The major drawback of this algorithm is its simplistic model which can address only frontal images with little expression variations and large non-facial regions. We wish to focus on a more high-quality enhancement of *facial* regions, and handle a variety of *subtle* expression variations.

Following this, Loke *et al.* [23] suggested to super-resolve very LR facial images by selecting a set of the most similar HR same-identity training images, in the sense of pose and expression. A similarity measure, based on pose estimation and an expression descriptor, relying on shape and texture, was used for selection. After aligning the selected images using triangulation and affine warping, patches of them were used to hallucinate the face using a MRF model, based on color and edge constraints and a smoothness term.

Drawbacks of this work include the selection process, based on a rough match of some facial regions to the query; we wish to handle more *subtle* expression variations. Replacing LR patches with HR ones results in noticeable artifacts, seams and change of color, since this patch-based method does not account for the human observer's sensitivity to certain facial regions and their expressions. Other drawbacks are using a very large HR dataset (thousands of images), their small size, and the manual labeling of feature points in the LR image.

## B. Insights

Previous works and early experiments point our important insights regarding facial images of a specific individual.

- The *non-rigid* behavior of faces and facial features under expression variation requires *non-rigid* registration, rather than affine. Most non-rigid methods do not use landmarks but pixels' intensities directly, since they need denser image information, and geometric landmarks are not invariant under non-rigid transformations [24]; e.g., locations of facial interest points under expression variations.
- As mentioned before, Joshi *et al.* observed that the space spanned by same-identity facial images, depicting a limited range of expressions, is significantly smaller than that spanned by multiple-identity images. Using *generic* faces as priors, on the other hand, introduces artifacts and possible changes in identity and expression.
- A change in identity or facial expression is visually very disturbing to a human observer. Therefore, only the most suitable examples, in the sense of shape, expression, gaze etc., should be used for reconstruction (This can also be deduced from [18], [22] and [23]).
- As Capel and Zisserman have observed, better learning is obtained when considering different facial regions, rather than *the whole face*. Loke *et al.*'s results demonstrate potential difficulties using a *patch-based* method, which does not take into account human observer sensitivity to certain facial regions and their expressions. Capel and Zisserman also noticed that better representation is needed when handling high-detail facial regions that

attract human attention and convey facial expression, such as eyes, compared to smooth regions, such as cheeks.

- Decomposing the face into facial regions increases the versatility in generating a variety of possible expressions, while decreasing the number of samples required. Since a certain "eye mode" (gaze, shape and closure) can be "accompanied" by many mouth expressions, this decomposition allows to construct and search datasets of small facial regions, rather than large whole-face images, saving both memory and computation time.

### C. The Proposed Method

In our work we use personal priors to enhance the quality of facial images of a particular person. We obtain new data-driven facial features spaces, based on only tens of high-quality, same-identity, same-pose example images, differing in facial expression; and define a new affinity measure to match them to given poor-quality images.

For each key facial feature (eye and mouth) and for different head poses, we construct a high-quality, identity-specific affinity space, representing various different "principal modes" of the specific feature, such as different eye gaze, closure and shape, or different mouth expressions (Fig. 5). This is done using a newly defined affinity measure for image matching under non-rigid variations, which derives from the distance between images, in the sense of the diffusion-based Demon transformation [25] required to register them.

This measure corresponds to the "visual validity" of images interpolated during the diffusion process: how natural, real-world they appear to a human observer. Fluid registration can also interpolate real-world looking images, that can expand the affinity space. Demon registration also provides a useful tool for fine registration of non-rigid facial features.

Given these identity-specific affinity spaces we enhance low-quality, same-identity facial images; specifically, dark cellular phone images degraded by unknown noise, resolution reduction, slight motion blur and color change. The measure's robustness to quality degradation enables to accurately match input facial features to the most similar example from the corresponding affinity space. Input facial regions are then replaced by the most suitable, Demon-registered, high-quality examples to obtain a high-quality facial image (Fig. 7).

## II. DEMON DIFFUSION-BASED AFFINITY SPACE

### A. Demon Diffusion-Based Fluid Registration

The Demon registration, first introduced by Thirion [25], [26], describes the gradual diffusion process of an object, represented by a deformable grid, into another object, represented by a semi-permeable membrane, through its boundaries by the action of Demon effectors.

Thirion showed the translation of this concept into a simple gradient-based displacement field  $\vec{u}$  from the *moving image*  $m$  to the *static image*  $s$ . The improvements suggested by Wang *et al.* [27] and Cachier *et al.* [24] yield the following:

$$\vec{u} = (m-s) \times \left( \frac{\vec{\nabla}s}{|\vec{\nabla}s|^2 + \alpha^2(s-m)^2} + \frac{\vec{\nabla}m}{|\vec{\nabla}m|^2 + \alpha^2(s-m)^2} \right) \quad (1)$$

where  $\vec{\nabla}$  denotes image gradient, and  $\alpha$  is a normalization factor accounting for adaptive force strength adjustment.

This registration method was so far usually used for medical image registration, such as the work of Kroon and Slump [28], whose implementation we use. A detailed explanation is given in Appendix A.

### B. Demon Diffusion-Based Affinity Measure

We construct an affinity measure to characterize the sequence of intermediate images generated during Demon diffusion (the "deformation path"), by its "visual validity": how natural, real-world and undistorted the path appears to a human observer (Fig. 2). We will show the resulting high correspondence between the measure and visual validity.

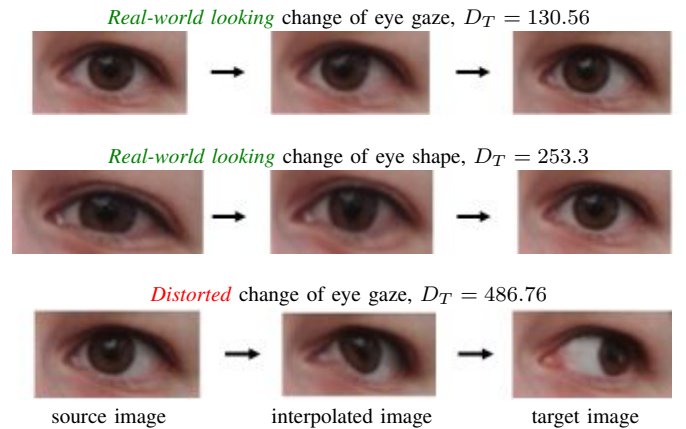


Fig. 2. Examples of deformation paths between high-quality eye images for identity #1, and their Demon measures. Compare the **low** Demon measure distances for the **visually valid** paths to the **higher** distance for the **visually non-valid** path.

To this end, we define a new Demon-based affinity measure (Eq. (2)) of the similarity between images under non-rigid variations. It is derived from the distance between images, in the sense of the Demon transformation required to register them. We use it as an affinity measure and matching criterion of different principal modes of the same facial feature.

The distance measure between two images is proportional to the mean absolute error between the *deformed* image  $m$  at a *fixed* time point  $T$  in the registration process (taken in our implementation as 200 iterations), and the target image  $s$ :

$$D_T(m, s, \alpha_l) = C \|m_{HSV, \alpha_l}(T) - s_{HSV, \alpha_l}\|_{L_1} \quad (2)$$

Where  $\alpha_l$  indicates feature-dependent HSV color space channel selection: hue channel for mouths, value channel for eyes. Intuitively, it is a measure of the distance "left to go" from  $m$  to  $s$ ; taking into consideration not only their naïve pixel-to-pixel similarity, but also Demon's *ability* to successfully deform one into another *in a given time* (as opposed to Cachier's minimization criterion, see Appendix A). It also relates to local structure and shape (as opposed to histogram distances or EMD, relating to *global*, non-spatial color information).

Given all these characteristics, it better reflects human visual judgment of visual validity, as perceived by a human observer, which can be roughly classified into two categories:



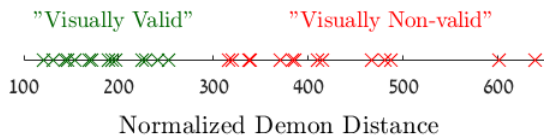


Fig. 3. Correspondence between visual validity and the (normalized) Demon distance (for eyes of identity #1). Compare the **lower** Demon distances, corresponding to the *visually valid* interpolated images, to the **higher** Demon distances, corresponding to the *visually non-valid* images.

- 1) *A visually valid deformation path.* Interpolated images along the deformation path appear as real-world images, describing intermediate phases in the gradual deformation process between images. This case corresponds to lower values of the quantitative distance.
- 2) *A visually non-valid deformation path.* Interpolated images along the deformation path appear distorted and cannot be considered as real-world facial features. This case corresponds to higher values of the distance.

Fig. 2 shows examples of deformation paths between high-quality eye images, and their Demon measures. It can be seen that the *visually valid*, real-world looking paths, depicting interesting, moderate variations, such as changes in eye gaze or shape, correspond to lower Demon distances; whereas the *visually non-valid*, distorted looking deformation path corresponds to a higher Demon distance.

Fig. 3 shows the correspondence between visual validity and the Demon distance for eye images of identity #1 (examples of which appear in Fig. 2). Visual validities of different deformation paths were determined using the concept described above. It can be seen that **lower values of the Demon distance correspond to visually valid deformation paths, and vice versa**; thus, different visual validity categories can be automatically differentiated using this measure. Note that we later use a nearest-neighbor scheme to choose the most relevant patch, so no actual threshold of validity should be chosen.

Appendix B shows a similar behavior when deforming synthetic images: for moderate variations, deformation succeeds and the measure *moderately* increases with variation. But for more drastic variations, the deformed image becomes too different or distorted; and the measure *drastically* increases.

Illumination consistency between images has much influence on Demon registration distortion (Fig. 4). Registering images similar in shape and structure, but differing in illumination, results in a distorted interpolated image, compared with the naturally-looking, same-structure, high-quality result obtained when a simple illumination adjustment (histogram equalization) is first used.

The measure cannot be considered as a distance or metric in the mathematical sense, as a triangle inequality cannot be shown.

A visually valid deformation path allows using the interpolated images as new real-world looking images, describing intermediate phases of subtle variations between existing principal modes, thus expanding considerably the available dataset. Finally, *Demon registration enables fine non-rigid registration*

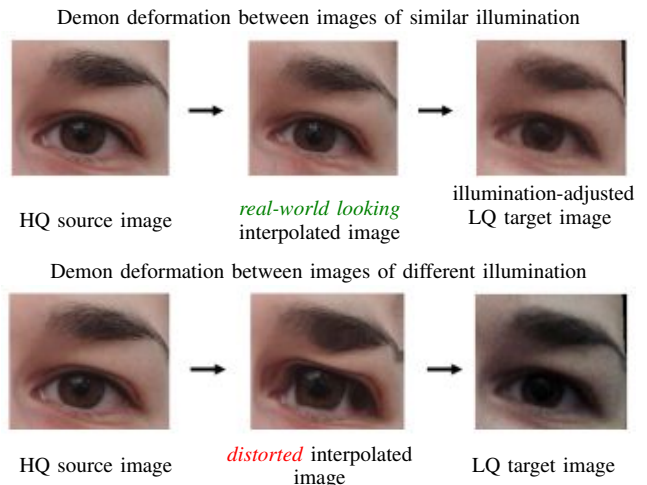


Fig. 4. Effect of illumination adjustment on Demon deformation: the naturally-looking, high-quality image obtained when deforming same-illumination images (top); compared to the distorted image obtained when deforming different-illumination images (bottom).

of facial features, needed to handle their non-rigid behavior under expression variations.

Concluding the Demon registration and measure important characteristics:

- 1) **Correspondence between Demon measure and visual validity:** As Demon registration relates to *shape and structure*, the deformed image reflects Demon's ability to handle non-rigid image variations, while preserving real-world appearance. As the Demon measure relates to Demon's ability to bring one image close to another, rather than their original distance, it corresponds to the visual validity of the deformed image resulting from registration. Therefore, *low Demon distances* correspond to *moderate non-rigid variations* between images, with *real-world appearance* of the interpolated images.
- 2) **Robustness to quality degradation:** Demon registration is quite robust to quality degradations, such as noise and resolution reduction, given that illumination is consistent; therefore, when registering HQ images to an LQ image, low distances still correspond to similar structures.
- 3) **Preserving source quality when registering different-quality images:** registering a HQ image to a similar-shape LQ image preserves its high quality, while adjusting to the desired shape, as can be seen in Fig. 4.

Combining these characteristics allows performing a measure-based Nearest Neighbor search to match a LQ query image to the most similar HQ dataset image, in the sense of Demon registration. The interpolated image resulting from registering the HQ match to the LQ query is of quite high-quality, naturally-looking and of desirable shape.

### C. Demon-Based Facial Features Affinity Spaces

Fig. 5 illustrates the concept of an affinity space based on the Demon-based affinity measure, with visually valid deformation paths between principal modes. A geodesic of interpolated,

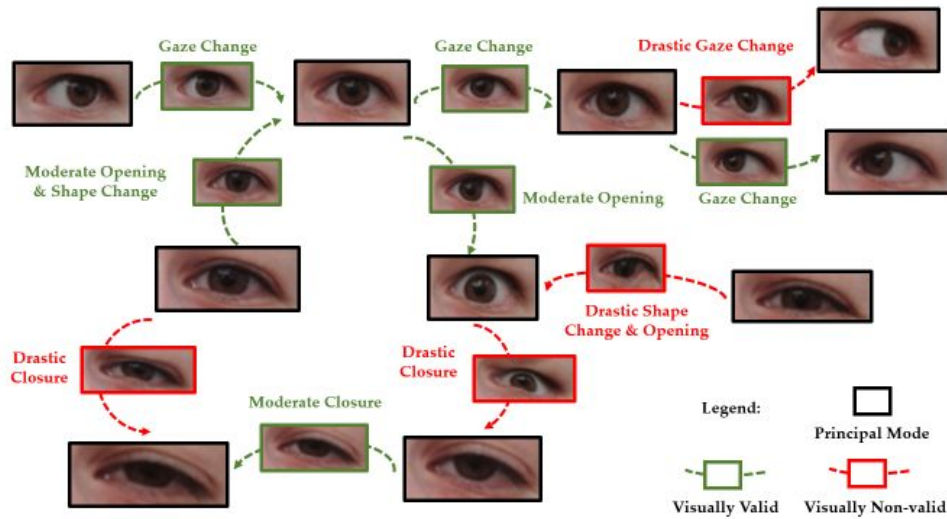


Fig. 5. Illustration of an eye affinity space, constructed based on the Demon-based affinity measure. Visually valid deformation paths and interpolated images appear in green, whereas visually non-valid ones appear in red.

visually valid images, depict intermediate steps in the deformation between images. Visually non-valid deformation paths are not allowed, since their interpolated images cannot be used to generate new visually valid images. Fig. 8 shows a real affinity space of same-identity, same-pose eyes, automatically constructed using the Demon affinity measure. Note that a non-frontal eye (uppermost right) wrongly classified as frontal during preprocessing (see Sec. III-A) is unconnected to all others. The affinity measure is used as a *matching criterion for choosing* an image from the dataset, which is the *most* similar to a given test image. **Note, that this search does not require knowledge of the connections between dataset images, or paths' visual validities.** As we have seen, the measure's robustness to image quality degradation allows finding the most suitable match even for a poor-quality query image.

We use only tens of personal priors images to *automatically* construct 14 data-driven spaces (2 identities with 2 poses each, one identity with 3 poses; for each pose, two spaces are constructed: for the left eye and for the mouth). Each space consists of multiple high-quality, same-identity, same-pose examples of a specific facial feature (about 20-30 principal modes per space). Fig. 6 shows examples of the personal priors image set. As opposed to previous works, affinity spaces describe many different *subtle* expression variations, such as different eye gaze, closure and shape, or different mouth closure, shape and expression.

In the future, it might be possible to use the subset of the most similar principal modes and the visually valid interpolated images between them as priors or constrains for other frameworks of image restoration. Another option might be to first get a rough notion of the relevant subset, using some kind of an initial "projection" of the degraded test image onto the space, thus making the selection process more time-efficient.

### III. FACIAL IMAGE QUALITY ENHANCEMENT

We now show the use of personal priors and the Demon concept for a semantically-aware enhancement of facial im-

ages. Fig. 7 illustrates the proposed method.

---

#### Algorithm 1: Facial Image Quality Enhancement.

---

**Data:** Degraded facial image (blind degradation model), HQ personal priors.

**Result:** Enhanced facial image.

- 1 Extract facial features, select relevant HQ patch affinity spaces according to identity and pose, Sec. III-A;
  - 2 For each semantic patch (eye, mouth): select the most similar HQ patch in the space, using illumination adjustment and Demon measure, Sec. III-B;
  - 3 Infer data for other facial regions from highly-correlated regions, Sec. III-C;
  - 4 Embed high-quality image details, using registration, color-correction and blending, Sec. III-D;
- 

The details of the algorithm are as follows:

#### A. Preprocessing: Facial Features Extraction

We use Zhu and Ramanan's algorithm [29] to detect the facial contour, whose convex hull is used as input to the image matting algorithm of Levin *et al.* [30]. Thresholding and erosion of the resulting mask (similar to the preprocessing in [22]) result in a head image, which will be later used for skin texture enhancement. We also use Zhu and Ramanan's pose estimation, to later search the suitable (same pose-sign) affinity spaces. For a more accurate facial landmarks localization we prefer using the algorithm of Asthana *et al.* [31], with the head image as the initial face detection. **Note, that HQ images are processed similarly for pose estimation, features and head extraction to construct the HQ spaces.**

#### B. NN Search using Affinity Measure

Nearest Neighbor searches through suitable (same pose-sign) affinity spaces are conducted to find the best matching



Fig. 6. Examples of our personal priors image set, which includes 7 sets of different identities and poses; each consists of 20-30 same-identity, same-pose, multiple-expression high-quality cellular images.

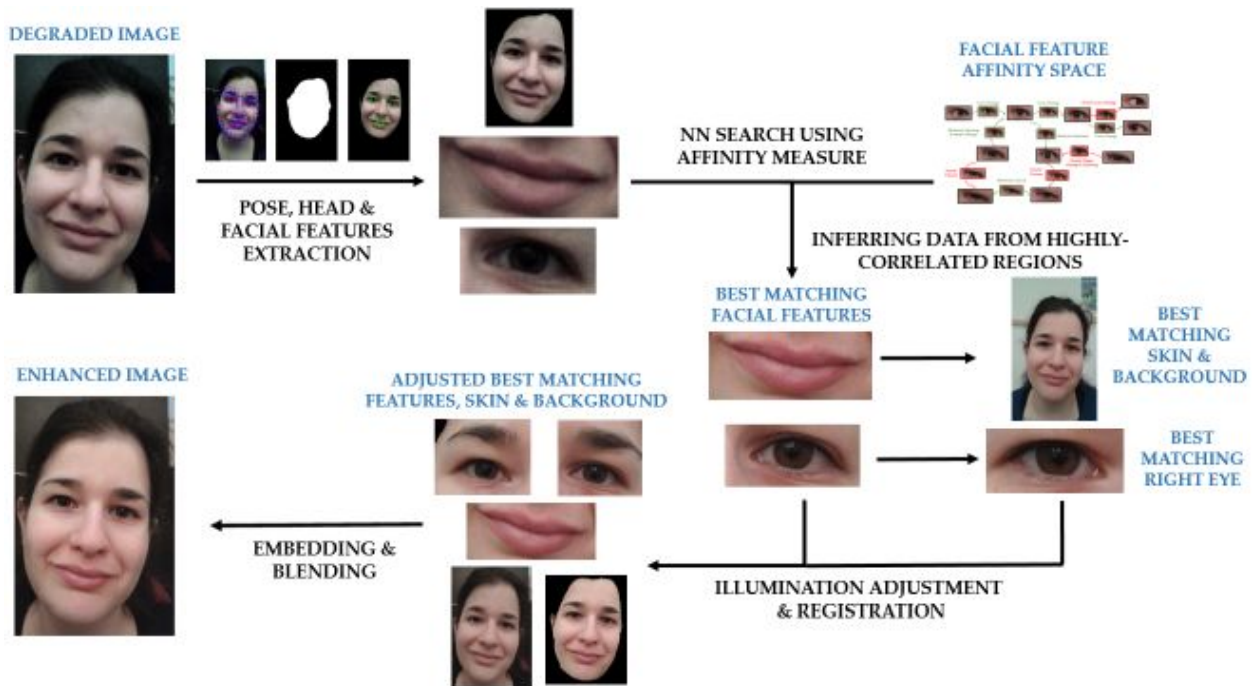


Fig. 7. Algorithm's flowchart: Facial image quality enhancement using the Demon-Based affinity measure and affinity spaces.

high-quality examples in the dataset. Throughout the search, **illumination adjustment** (using histogram equalization) is performed prior to distance calculation.

### C. Inferring Data from Highly-correlated Regions

For facial image enhancement, structure and context correlations between semantically meaningful face regions, used as building blocks, are used to infer the suitable data. To select the proper *right* eye, based on the *left* eyes space, we make the reasonable assumption of gaze, closure and shape consistency between both eyes (ignoring cross-eye and winking). This allows to extract the suitable right eye from *the same high-quality image from which the left eye example was taken*. Thus, avoiding the need to construct a right eyes space.

Another use of facial semantic structural constrains regards head structure and skin texture. In general, the shape of middle-low facial regions (cheeks, chin, facial lower contour and even nose) depends on the mouth expression, but remains unchanged under eye expression variations. Therefore, given the large collection of available high-quality images, it is only reasonable to use *the same high-quality image from which the*

*mouth was taken* to also extract skin information. Therefore, a high-quality background image, head structure and skin texture information are selected according to best matching mouth.

### D. Embedding High-quality Image Details

The **input image and input head/skin** undergo **illumination adjustment** to the brighter illumination of the selected high-quality background image and example head/skin image, respectively, using the NRDC algorithm [32]. Due to the randomized nature of Generalized PatchMatch embedded in NRDC, we choose out of several repetitions the best illuminated background, *in the sense of its NIQE score* [33] (see Sec. IV). The **example head/skin** image undergoes affine **registration** to best fit the input. As to the **facial features**, input features undergo **illumination adjustment** to the brighter high-quality illumination. Then, example features undergo **fine non-rigid registration** to best fit the input feature structure.

Finally, we embed the high-quality skin texture and facial features information into the brighter noisy image, using Burt and Adelson's multi-resolutional **blending** [34] to produce a seamless, smooth appearance.



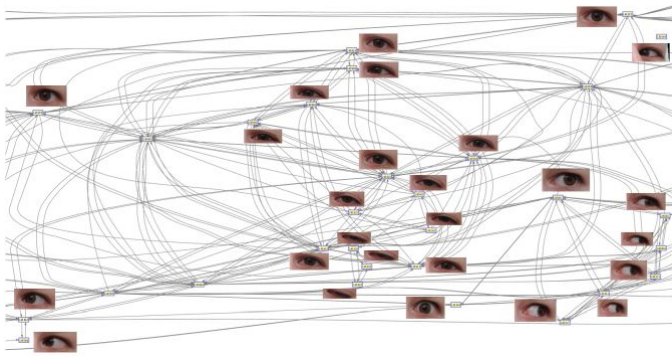


Fig. 8. Example of a real affinity space of same-identity, same-pose eyes, automatically constructed using the Demon affinity measure.

IV. EXPERIMENTAL RESULTS

We now show experimental results for our prior-based denoising and quality enhancement algorithm. Input facial images were taken using a SAMSUNG GT-S7580L cellular frontal camera (2560X1536 resolution) in a dark environment. Assuming no known information regarding the camera’s specifications and built-in image processing algorithms. This real life scenario of dark environment cellular shooting demonstrates well common flaws of shot noise, post-processed by unknown (possibly nonlinear) filtering, slight motion blur and resolution reduction of unknown parameters. Prior and input images were downsampled by a factor of 2 before processing. Using an unoptimized Matlab code with Matlab/C++ code segments, on a Windows 7 OS, Intel i7-4770 CPU at 3.4 GHz with 16GB RAM, the running time using a single NRDC-NIQE iteration was 3 minutes; running time was 4 minutes when using 5 iterations.

We demonstrate our results for multiple identities, poses and expressions, visually comparing them to the prior-based brightened image using NRDC, and a state-of-the-art BM3D [7] denoising of the brightened image, assuming AGW noise of  $\text{std}=10$ . Since **no ground truth images are available**, we use the *no-reference* blind-model image quality assessment score NIQE [33] to quantitatively compare the methods. The NIQE score better suits unconstrained environments such as ours, as it measures deviations from natural image statistics, rather than tuning to specific distortions by training. Each example displays the NIQE scores of the processed images, normalized to the NIQE score of the high-quality image found. As the NIQE score *decreases* as quality *increases*, **the closer the score is to 1 - the better the quality**.

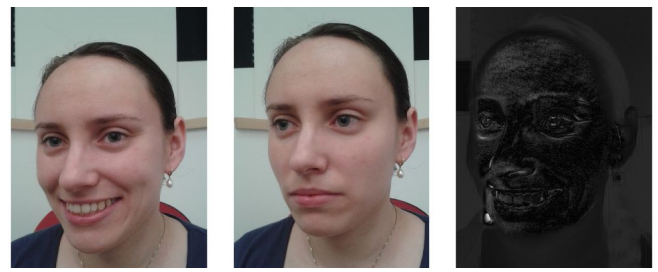
It can be easily seen for all examples, both visually and quantitatively, that our algorithm yields better results than either the input dark image, the brightened noisy image or the BM3D denoised one. It does not only remove noise, but also embeds new HQ details, while preserving pose, expression and identity. Table I and Fig. 11 show that it outperforms the prior-based brightening method, which outperforms the input; BM3D processing is always worse than the input (one should note though, that using BM3D in such a blind model is quite far from the standard denoising model of AWGN with known noise variance, where BM3D performs very well).



(a) Low quality input image, NIQE score=1.2032 (b) Prior-based brightened input image, NIQE score=1.1058



(c) BM3D Denoising of brightened image, estimated noise  $\text{std}=10$ , NIQE score=1.6097 (d) Proposed method, NIQE score=1.0187



(e) HQ exmple for mouth & head info. and background illumination (f) HQ exmple for eyes info. (g) Difference image: Brightened input to our result



Brightened input BM3D Denoising Proposed method

Fig. 9. Denoising and quality enhancement example.

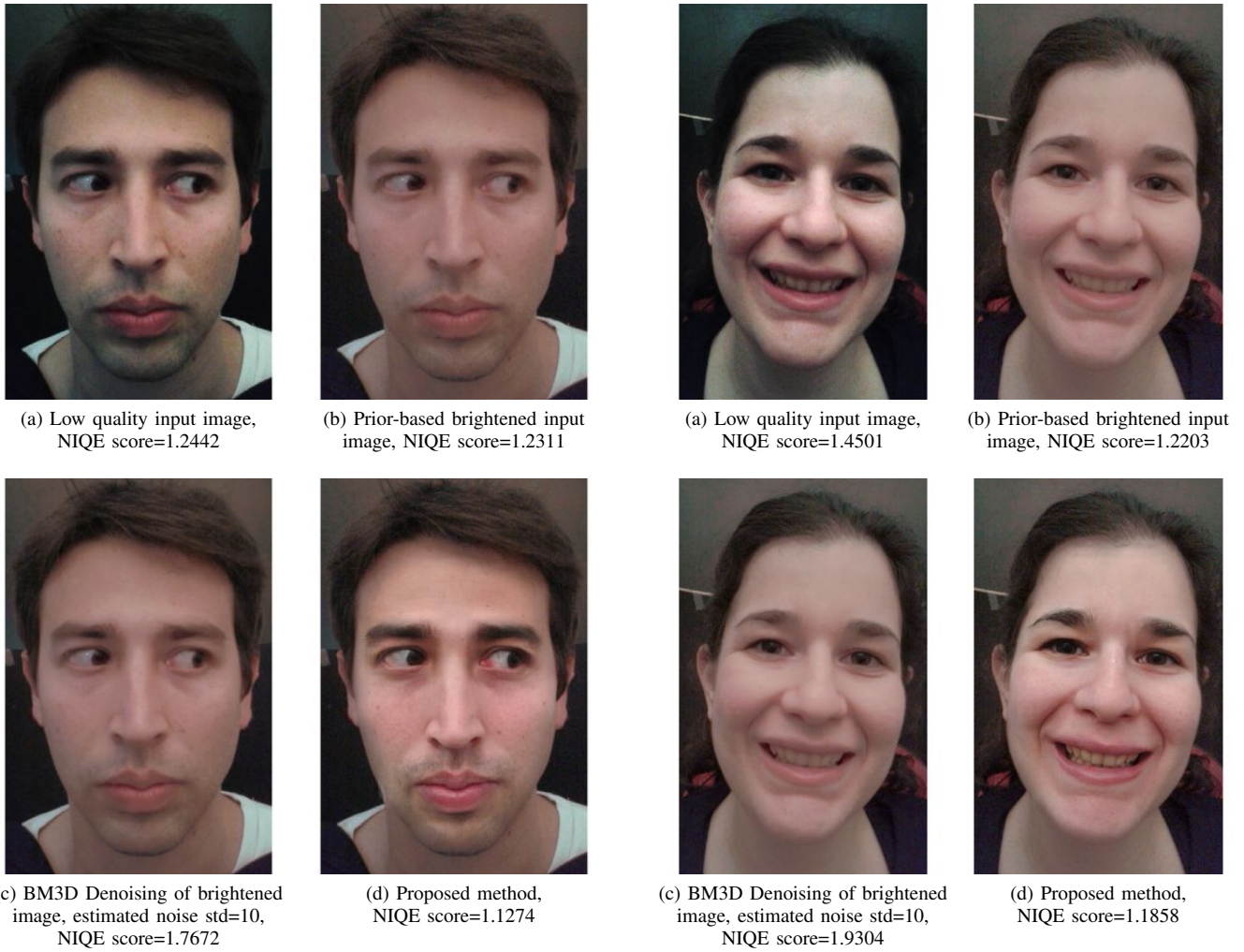


Fig. 10. Denoising and quality enhancement example.

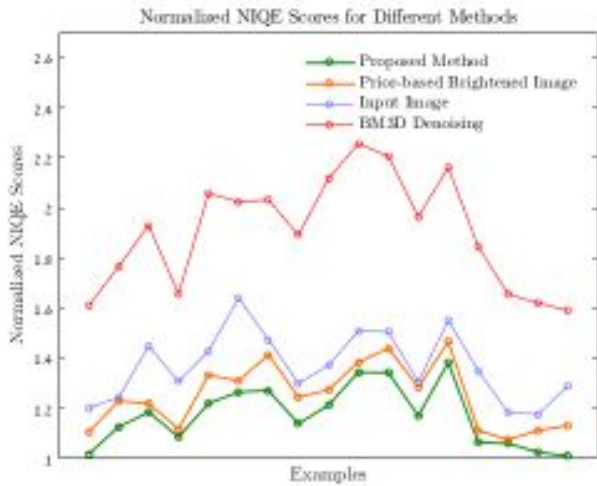


Fig. 11. Normalized NIQE scores for different methods for 17 examples. **The closer the normalized score is to 1 - the better the quality.** Therefore it can be seen that **our method** outperforms **the prior-based brightening method**; which outperforms **the input image**; which outperforms **BM3D**.

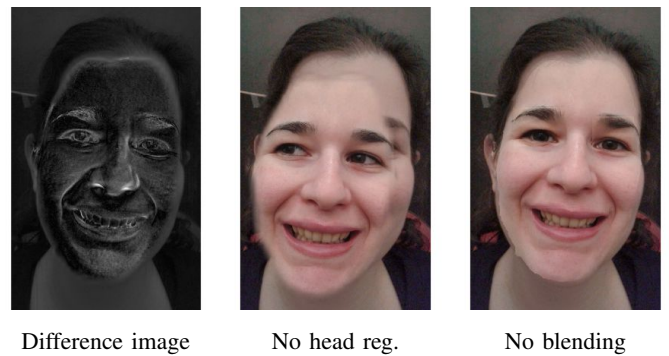


Fig. 12. Denoising and quality enhancement example.

TABLE I  
NORMALIZED NIQE QUALITY ASSESSMENT FOR DIFFERENT METHODS

	Proposed method	Prior-based brightened image	Input image	BM3D Denoising
Average score	<b>1.1729</b>	1.2512	1.3708	1.9056
Relative imp. over input [%]	<b>14.43</b>	8.72	0	-39.02

Difference images between prior-based brightened input



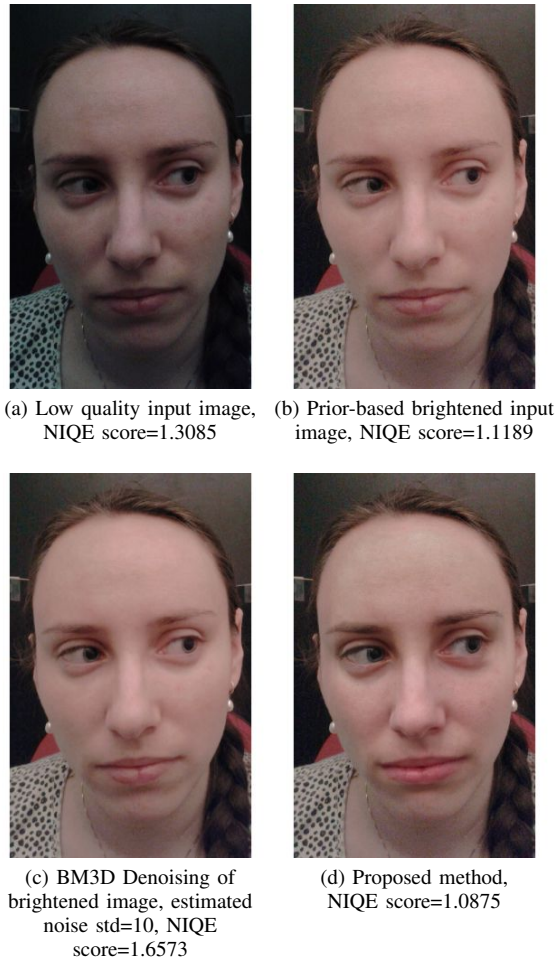


Fig. 13. Denoising and quality enhancement example.

images and our results (Figs. 9, 12) show how using personal priors not only removes noise, but also embeds image details and fine textures, e.g. in the eyes, eyebrows and mouth. Fig. 9 also shows a close-up comparison of significant facial regions (that attract human attention and convey facial expression) for different methods. In addition, it displays the high-quality example images used to extract prior information: the image used to extract mouth & head/skin information and for background illumination adjustment; and the image used to extract eyes information. Note that the mouth/head example is similar in pose and mouth expression to the input, but different in eye expression, background, hair, clothes, etc.

In Fig. 12, 14 we discuss the effect of errors or omission of certain stages in the algorithm. Fig. 12 shows the necessity of the head registration and blending stages for visually reasonable results. Fig. 14 shows the effect of erroneous example facial feature selection (relating to the example in Fig. 7). The Demon measure allows accurate selection. But what if the selection process resulted in errors? These could have been caused, for instance, by insufficient expression variations in the dataset; or when skipping the illumination adjustment phase (see Fig. 4). Demon registration's **robustness to moderate non-rigid variations** allows it to overcome moderate selection errors, such that the resulting interpolated features are of quite

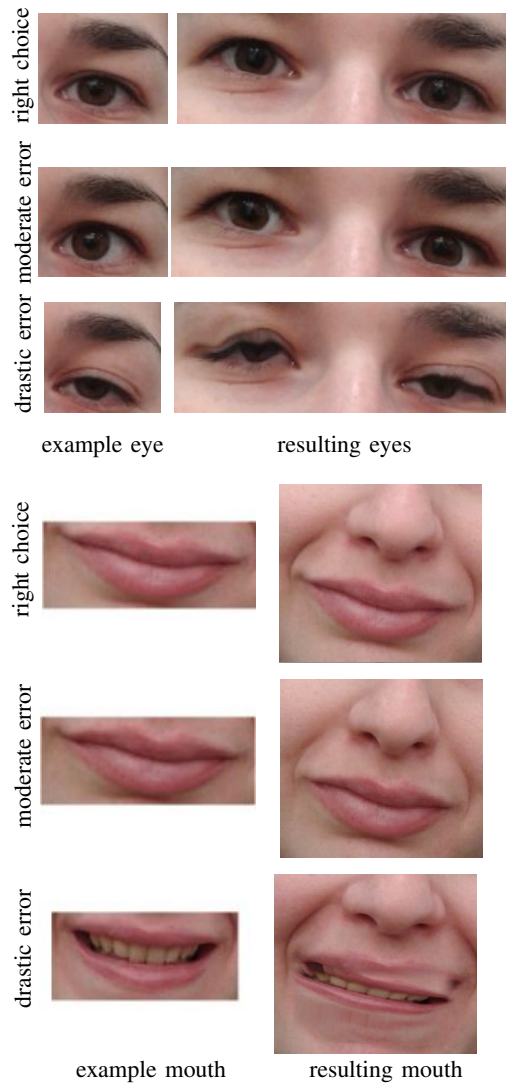
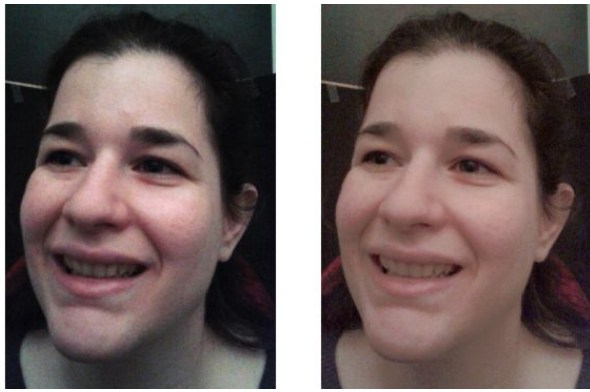


Fig. 14. The Demon measure **allows accurate selection** of example facial features. **But what if the selection process resulted in errors?** Demon registration's **robustness to moderate non-rigid variations** allows it to **overcome moderate selection errors**, such that the resulting interpolated features are of quite desirable shape. However, more drastic errors result in severely distorted features. Examples relate to the example in Fig. 7.

desirable shape, but somewhat distorted. However, features interpolated using very wrongly selected examples display wrong and distorted expressions. Note the wrong nose and wrinkles when wrongly selecting the mouth expression.

## V. CONCLUSION

In this work we aim to overcome classical image processing limits by combining semantic patches and registration methods for visual image enhancement. We demonstrate our method for the problem of cellular photography enhancement of dark facial images. Given today's easily available photography devices, our model assumes that high-quality personal priors are available, but that we are blind to the degradation model and its parameters. A low-to-moderate degradation may include an unknown mix of noise, nonlinear post-processing artifacts, certain motion blur, resolution reduction and color-change. The blind model assumption allows a very general correction



(a) Low quality input image, NIQE score=1.4289  
(b) Prior-based brightened input image, NIQE score=1.3338



(c) BM3D Denoising of brightened image, estimated noise std=10, NIQE score=2.0586  
(d) Proposed method, NIQE score=1.2209

Fig. 15. Denoising and quality enhancement example.

mechanism which is not device and scenario dependent. In order to solve this we use non-rigid semantic patches and a registration algorithm, which is robust to noise and blur, and can infer a high quality solution based on the priors.

The experimental results demonstrate how our method achieves significant quality enhancement over the degraded input images, both visually and quantitatively, based on the no-reference NIQE measure. Our building blocks are facial features of coherent structure and context with adaptive size and location. A new affinity measure is defined based on the non-rigid, diffusion-based Demon registration. We use it to construct data-driven, high-quality facial features spaces, representing various expression variations.

The measure's robustness to image quality degradation and non-rigid variations allows accurate matches of low-quality features to high-quality examples. This enables high enhancement quality, relying on only tens of personal priors, maintaining well the person's features and facial expressions. In a future work we consider processing of more abstract non-facial data within a generalized framework.

#### APPENDIX A DEMON REGISTRATION

The Demon registration is a diffusion-based image registration algorithm, approximating fluid registration, based on



(a) Low quality input image, NIQE score=1.6402  
(b) Prior-based brightened input image, NIQE score=1.312



(c) BM3D Denoising of brightened image, estimated noise std=10, NIQE score=2.025  
(d) Proposed method, NIQE score=1.2658

Fig. 16. Denoising and quality enhancement example.

polarity. It uses the transformation field caused by edge-based forces. It was first introduced by Thirion [25], [26] as an analogy of Maxwell's "Demons" in a paradox of thermodynamics.

Fig. 17, taken from Thirion's work [26], shows the Demon diffusion process. An object in the deforming image, referred to as "the moving image", is represented by a deformable grid, whose nodes are labeled "inside" or "outside"; their inner relations correspond to object rigidity. The boundaries of an object in the other image, referred to as "the static image", are represented by a semi-permeable membrane, along which Demon effectors are situated. The deformable grid gradually

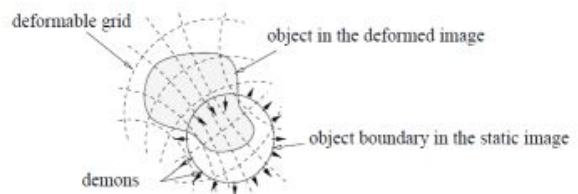
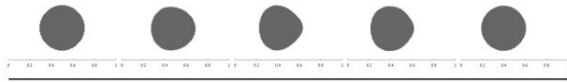
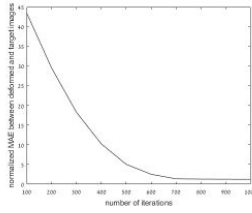


Fig. 17. Demon diffusion process [26]: the "moving" object, represented by a deformable grid, diffuses through a semi-permeable membrane representing the boundaries of the "static" object, by the action of Demon effectors.

diffuses into the static object through its boundaries by the action of these effectors. Diffusion is guided by the principle of polarity, that is, maximal common polarity at each side of



(a) From left to right: original image and intermediate images generated for 200, 400, 500 and 700 iterations.



(b) Mean absolute error between deformed and target images vs. number of iterations

Fig. 18. Intermediate steps in the diffusion process for object translation.



(a) From circle to square.

(b) From square to circle.

Fig. 19. Deformation of a circle to a square, and vice versa (for 200 iterations). Left: source image. Middle: deformed image. Right: target image.

the membrane: Demon effectors act to locally "push" nodes labeled "inside" through the membrane interface into the static object, and vice versa. To this end, Demons might use spatial location, direction, pixel intensity or other information.

The final transformation results from iteratively evolving a family of transforms under two types of forces: "internal" forces, reflecting inner relations between neighboring image points, corresponding to image rigidity; and "external" forces, reflecting interaction between the static and moving images.

Fig. 18 illustrates this, showing the intermediate steps of diffusing an object into a same-shape translated object, until perfect registration is achieved (Fig. 18a), and the mean absolute error between deformed and target images as a function of the number of iterations (Fig. 18b). Fig. 19 demonstrates the difficulty in deforming a high-curvature shape into a low-curvature shape *in a given time*, and vice versa.

Thirion [25] showed the translation of this concept into a simple gradient-based displacement field  $\vec{u}$ , to estimate the displacement of a pixel in the *moving image*  $m$ , required to match the corresponding point in the *static image*  $s$ .

Denoting pixel intensity as a function of time:  $i(x(t), y(t), z(t), t)$ , differentiating the instantaneous optical flow equation gives:

$$\frac{\partial i}{\partial x} \frac{\partial x}{\partial t} + \frac{\partial i}{\partial y} \frac{\partial y}{\partial t} + \frac{\partial i}{\partial z} \frac{\partial z}{\partial t} = - \frac{\partial i}{\partial t} \quad (3)$$

Considering that the evolution in one time unit is the difference between images:  $\frac{\partial i}{\partial t} = s - m$ , and  $\vec{u} = (\frac{dx}{dt}, \frac{dy}{dt}, \frac{dz}{dt})$  is the instantaneous velocity from  $m$  to  $s$ , we get:

$$\vec{u} \cdot \vec{\nabla} s = m - s \quad (4)$$

where  $\vec{\nabla}$  denotes image gradient. Defining  $\vec{\nabla} s$  as the internal edge-based force, and  $(m - s)$  as the external force,  $\vec{u}$  is

computed locally as the shortest translation of a point of  $m$  onto the hyperplane approximating  $s$ :

$$\vec{u} = \frac{(m - s) \vec{\nabla} s}{|\vec{\nabla} s|^2} \quad (5)$$

Unfortunately, small intensity variations can result in infinite Demon forces. To stabilize the resulting unstable equation:

$$\vec{u} = \frac{(m - s) \vec{\nabla} s}{|\vec{\nabla} s|^2 + (m - s)^2} \quad (6)$$

To improve stability and convergence speed, Wang *et al.* [27] added an "active force". Diffusion was considered a bi-directional process, and therefore Demon effectors also produced an internal gradient-based force of  $m$ , that diffuses  $s$  into  $m$ . A normalization factor  $\alpha$  is used to account for the adaptive force strength adjustment (suggested by Cachier *et al.* [24]), yielding the following displacement field:

$$\vec{u} = (m - s) \times \left( \frac{\vec{\nabla} s}{|\vec{\nabla} s|^2 + \alpha^2 (s - m)^2} + \frac{\vec{\nabla} m}{|\vec{\nabla} m|^2 + \alpha^2 (s - m)^2} \right) \quad (7)$$

The simple, iterative Demon registration algorithm introduced by Wang *et al.* consists of the following steps:

- 1) Calculation of the disp. field using Eq. (7).
- 2) Regularization of the disp. field using Gaussian smoothing, to suppress noise and preserve geometric continuity.
- 3) Adding the regularized disp. field to the total disp. field.
- 4) Image deformation according to the total disp. field.

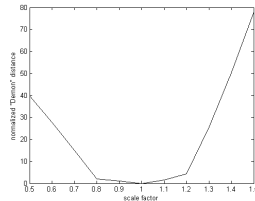
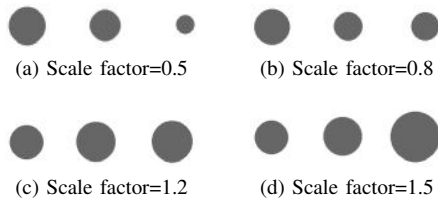
Cachier *et al.* showed in their work that the Demon algorithm can be seen as an approximation of a second order gradient descent of a SSD criterion, and proposed using this criterion to compare different non-rigid registration methods. But, as opposed to our work, it was not used as an affinity criterion or to evaluate the success of image deformation.

This registration method was so far usually used for medical image registration, such as the work of Kroon and Slump [28].

Another non-rigid registration, penalizing mismatch between deformed and target images, is optimal mass transport, finding the cheapest mass transport path, by minimizing the L2 Kantorovich-Wasserstein distance. Benamou and Brenier [35] proved it can be *reformulated as a fluid mechanics problem*.

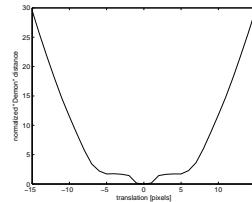
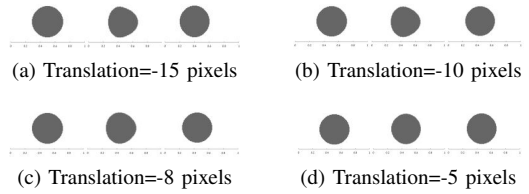
As far as we know, optimal transport or other fluid methods haven't been used so far in a framework similar to ours; but, some existing works do relate to ours. Haker *et al.* [36] used OT for image registration, aiming to achieve the minimal possible distance, while interpolating intermediate images (interpolation was also done by Kerrache and Nakauchi [37]). This is as opposed to our *time-limited* process aimed to determine *visual validity*-related affinities between images. Wang *et al.* [38] used a *linear* approximated framework to quantify and visualize variations in a set of images; but their image approximation becomes less accurate as images become less sparse, and might not suit our needs. Kolouri and Rohde [39] represented displacement fields between *multiple-identity* HR facial images as *linear* combinations of basis fields, to constrain a super-resolution procedure. And last, Hassanien and Nakajima [40] used the PDE-based Navier elastic body splines





(e) Demon distance as a function of scale factor

Fig. 20. Demon deformation for object scaling at different factors. For each scale factor (a)-(d): Left: source image. Middle: deformed image. Right: target image, that is, the source image scaled.



(e) Demon distance as a function of translation

Fig. 21. Demon deformation for different object translations. For each translation (a)-(d): Left: source image. Middle: deformed image. Right: target image, that is, the source image translated.

for morphing and interpolation between *multiple-identity* facial images, but their method requires knowledge of feature points and their correspondences.

APPENDIX B

VALID AND NON-VALID DEMON DEFORMATION EXAMPLES

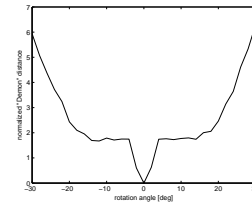
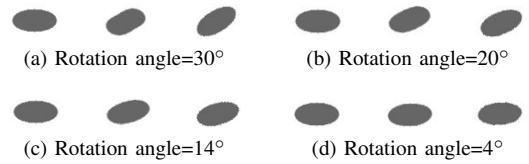
We demonstrate the behavior of *time-limited* Demon deformation and measure (using 200 iterations), under basic affine transformations. Fig. 20 demonstrates the *visual* success of the deformation and measure for different scale variations. Note, that changing scale involves the dis/appearance of mass. Similarly, Fig. 21 and 22 display the behavior for different translations or rotation angles, respectively.

These experiments all illustrate the same behavior: for moderate variations the *time-limited* Demon deformation succeeds: the deformed image gets as close as possible to the target image (practically identical) (Figs. 20b, 20c, 21d, 22c, 22d); and the Demon measure *moderately* increases with variation. But there exists a breaking point where the *time-limited* deformation starts to fail: the deformed image is too different from the target image, or distorted (Figs. 20a, 20d, 21a to 21c, 22a, 22b); and the measure starts to *drastically* increase.

We also explore this behavior for a common non-rigid facial expression deformation: a change in eye gaze (Fig. 23). As seen before, moderate variations in eye gaze result in successful deformations and a moderate increase in Demon distance (Figs. 23c, 23d), whereas greater variations result in *distorted* images and a drastic increase in distance (Figs. 23a, 23b). Fig. 23e compares the same breaking-point behavior seen before, to the *linear* behavior of the MAE between *source* and target images, not reflecting the deformation’s success.

ACKNOWLEDGMENT

The authors would like to thank Yossi Bar Erez, Raz Nossek and Alona Baruhov for their assistance.



(e) Demon distance as a function of rotation angle

Fig. 22. Demon deformation for object rotation at different angles. For each rotation angle (a)-(d): Left: source image. Middle: deformed image. Right: target image, that is, the source image rotated.

REFERENCES

- [1] B. K. Horn and B. G. Schunck, “Determining optical flow,” in *1981 Technical symposium east*. International Society for Optics and Photonics, 1981, pp. 319–331.
- [2] D. Geman and G. Reynolds, “Constrained restoration and the recovery of discontinuities,” *IEEE Transactions on Pattern Analysis & Machine Intelligence*, no. 3, pp. 367–383, 1992.
- [3] L. I. Rudin, S. Osher, and E. Fatemi, “Nonlinear total variation based noise removal algorithms,” *Physica D: Nonlinear Phenomena*, vol. 60, no. 1, pp. 259–268, 1992.
- [4] J. Huang and D. Mumford, “Statistics of natural images and models,” in *Computer Vision and Pattern Recognition, 1999. IEEE Computer Society Conference on.*, vol. 1. IEEE, 1999.
- [5] E. P. Simoncelli, “Bayesian denoising of visual images in the wavelet domain,” in *Bayesian inference in wavelet-based models*. Springer, 1999, pp. 291–308.
- [6] A. Buades, B. Coll, and J.-M. Morel, “A review of image denoising algorithms, with a new one,” *Multiscale Modeling & Simulation*, vol. 4, no. 2, pp. 490–530, 2005.
- [7] K. Dabov, A. Foi, V. Katkovnik, and K. Egiazarian, “Color image denoising via sparse 3d collaborative filtering with grouping constraint in luminance-chrominance space,” in *Image Processing, 2007. ICIP 2007. IEEE International Conference on.*, vol. 1. IEEE, 2007, pp. 1–313.

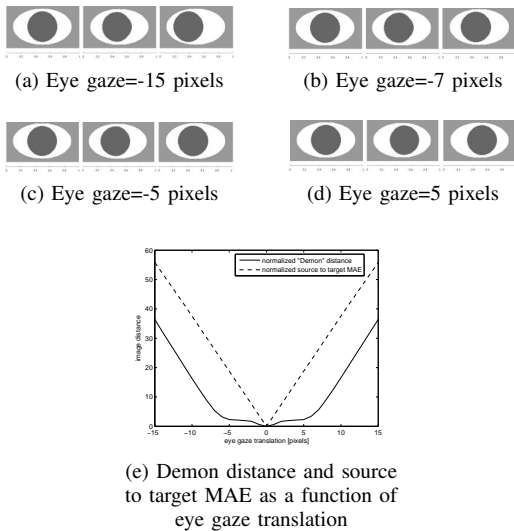


Fig. 23. Demon deformation for different eye gaze translations. For each translation (a)-(d): Left: source image, depicting a central gaze. Middle: deformed image. Right: target image, depicting a gaze change.

- [8] S. Roth and M. J. Black, "Fields of experts: A framework for learning image priors," in *Computer Vision and Pattern Recognition, 2005. CVPR 2005. IEEE Computer Society Conference on*, vol. 2. IEEE, 2005, pp. 860–867.
- [9] M. Aharon, M. Elad, and A. Bruckstein, "K-SVD: An Algorithm for Designing Overcomplete Dictionaries for Sparse Representation," *Signal Processing, IEEE Transactions on*, vol. 54, no. 11, pp. 4311–4322, 2006.
- [10] Y. Chen, W. Yu, and T. Pock, "On learning optimized reaction diffusion processes for effective image restoration," in *Proceedings of the IEEE Conference on Computer Vision and Pattern Recognition, 2015*, pp. 5261–5269.
- [11] H. Talebi and P. Milanfar, "Asymptotic performance of global denoising," *SIAM Journal on Imaging Sciences*, vol. 9, no. 2, pp. 665–683, 2016.
- [12] Y. Romano and M. Elad, "Boosting of image denoising algorithms," *SIAM Journal on Imaging Sciences*, vol. 8, no. 2, pp. 1187–1219, 2015.
- [13] S. Baker and T. Kanade, "Limits on super-resolution and how to break them," *Pattern Analysis and Machine Intelligence, IEEE Transactions on*, vol. 24, no. 9, pp. 1167–1183, 2002.
- [14] A. Levin and B. Nadler, "Natural image denoising: Optimality and inherent bounds," in *Computer Vision and Pattern Recognition (CVPR), 2011 IEEE Conference on*. IEEE, 2011, pp. 2833–2840.
- [15] S. Baker and T. Kanade, "Hallucinating faces," in *Automatic Face and Gesture Recognition, 2000. Proceedings. Fourth IEEE International Conference on*. IEEE, 2000, pp. 83–88.
- [16] O. Bryt and M. Elad, "Compression of facial images using the k-svd algorithm," *Journal of Visual Communication and Image Representation*, vol. 19, no. 4, pp. 270–282, 2008.
- [17] D. Capel and A. Zisserman, "Super-resolution from multiple views using learnt image models," in *Computer Vision and Pattern Recognition, 2001. CVPR 2001. Proceedings of the 2001 IEEE Computer Society Conference on*, vol. 2. IEEE, 2001, pp. II–627.
- [18] K. Jia and S. Gong, "Generalized face super-resolution," *Image Processing, IEEE Transactions on*, vol. 17, no. 6, pp. 873–886, 2008.
- [19] K.-C. Lee, J. Ho, M.-H. Yang, and D. Kriegman, "Video-based face recognition using probabilistic appearance manifolds," in *Computer Vision and Pattern Recognition, 2003. Proceedings. 2003 IEEE Computer Society Conference on*, vol. 1. IEEE, 2003, pp. I–313.
- [20] J. Yu, B. Bhanu, Y. Xu, and A. K. Roy-Chowdhury, "Super-resolved facial texture under changing pose and illumination," in *Image Processing, 2007. ICIP 2007. IEEE International Conference on*, vol. 3. IEEE, 2007, pp. III–553.
- [21] Y. Shih, V. Kwatra, T. Chinen, H. Fang, and S. Ioffe, "Joint noise level estimation from personal photo collections," in *Computer Vision (ICCV), 2013 IEEE International Conference on*. IEEE, 2013, pp. 2896–2903.
- [22] N. Joshi, W. Matusik, E. H. Adelson, and D. J. Kriegman, "Personal photo enhancement using example images," *ACM Trans. Graph.*, vol. 29, no. 2, p. 12, 2010.
- [23] Y. R. Loke, P. Tan, and A. A. Kassim, "Face hallucination on personal photo albums," in *Computer Vision-ACCV 2012 Workshops*. Springer, 2013, pp. 284–295.
- [24] P. Cachier, X. Pennec, and N. Ayache, "Fast non rigid matching by gradient descent: Study and improvements of the "demons" algorithm," 1999.
- [25] J.-P. Thirion, "Fast non-rigid matching of 3d medical images," 1995.
- [26] —, "Image matching as a diffusion process: an analogy with maxwell's demons," *Medical image analysis*, vol. 2, no. 3, pp. 243–260, 1998.
- [27] H. Wang, L. Dong, J. O'Daniel, R. Mohan, A. S. Garden, K. K. Ang, D. A. Kuban, M. Bonnen, J. Y. Chang, and R. Cheung, "Validation of an accelerated 'demons' algorithm for deformable image registration in radiation therapy," *Physics in medicine and biology*, vol. 50, no. 12, p. 2887, 2005.
- [28] D.-J. Kroon and C. H. Slump, "Mri modality transformation in demon registration," in *Biomedical Imaging: From Nano to Macro, 2009. ISBI'09. IEEE International Symposium on*. IEEE, 2009, pp. 963–966.
- [29] X. Zhu and D. Ramanan, "Face detection, pose estimation, and landmark localization in the wild," in *Computer Vision and Pattern Recognition (CVPR), 2012 IEEE Conference on*. IEEE, 2012, pp. 2879–2886.
- [30] A. Levin, D. Lischinski, and Y. Weiss, "A closed-form solution to natural image matting," *Pattern Analysis and Machine Intelligence, IEEE Transactions on*, vol. 30, no. 2, pp. 228–242, 2008.
- [31] A. Asthana, S. Zafeiriou, S. Cheng, and M. Pantic, "Incremental face alignment in the wild," in *Proceedings of the IEEE Conference on Computer Vision and Pattern Recognition, 2014*, pp. 1859–1866.
- [32] Y. HaCohen, E. Shechtman, D. B. Goldman, and D. Lischinski, "Non-rigid dense correspondence with applications for image enhancement," *ACM transactions on graphics (TOG)*, vol. 30, no. 4, p. 70, 2011.
- [33] A. Mittal, R. Soundararajan, and A. C. Bovik, "Making a completely blind image quality analyzer," *Signal Processing Letters, IEEE*, vol. 20, no. 3, pp. 209–212, 2013.
- [34] P. J. Burt and E. H. Adelson, "A multiresolution spline with application to image mosaics," *ACM Transactions on Graphics (TOG)*, vol. 2, no. 4, pp. 217–236, 1983.
- [35] J.-D. Benamou and Y. Brenier, "A computational fluid mechanics solution to the monge-kantorovich mass transfer problem," *Numerische Mathematik*, vol. 84, no. 3, pp. 375–393, 2000.
- [36] S. Haker, L. Zhu, A. Tannenbaum, and S. Angenent, "Optimal mass transport for registration and warping," *International Journal of computer vision*, vol. 60, no. 3, pp. 225–240, 2004.
- [37] S. Kerrache and Y. Nakauchi, "Interpolation between images by constrained optimal transport," in *VISAPP, 2011*, pp. 75–84.
- [38] W. Wang, D. Slepčev, S. Basu, J. A. Ozolek, and G. K. Rohde, "A linear optimal transportation framework for quantifying and visualizing variations in sets of images," *International journal of computer vision*, vol. 101, no. 2, pp. 254–269, 2013.
- [39] S. Kolouri and G. K. Rohde, "Transport-based single frame super resolution of very low resolution face images," in *Proceedings of the IEEE Conference on Computer Vision and Pattern Recognition, 2015*, pp. 4876–4884.
- [40] A.-E. Hassanien and M. Nakajima, "Image morphing of facial images transformation based on navier elastic body splines," in *Computer Animation 98. Proceedings*. IEEE, 1998, pp. 119–125.

**Ester Hait** received her B.Sc. degree in Electrical Engineering (Cum Laude) from the Technion, Haifa, Israel, in 2014. She is currently pursuing her M.Sc. degree in Electrical Engineering in the Technion. Her research interests include image processing and computer vision.

**Guy Gilboa** is a faculty member at the Department of Electrical Engineering, Technion - Israel Institute of Technology, since 2013.